Journal of Korea TAPPI
Vol. 32. No. 5, 2000
Printed in Korea

Characterization of the Spatial Variability of Paper Formation Using a Continuous Wavelet Transform

D. Steven Keller, Philip Luner, and Joel J. Pawlak

ABSTRACT

In this investigation, a wavelet transform analysis was used to decompose beta-radiographic formation images into spectral and spatial components. Conventional formation analysis may use spectral analysis, based on Fourier transformation or variance vs. zone size, to describe the grammage distribution of features such as flocs, streaks and mean fiber orientation. However, these methods have limited utility for the analysis of statistically stationary data sets where variance is not uniform with position, e.g. paper machine CD profiles (especially those that contain streaks). A continuous wavelet transform was used to analyze formation data arrays obtained from radiographic imaging of handsheets and cross machine paper samples. The response of the analytical method to grammage, floc size distribution, mean fiber orientation and sensitivity to feature localization were assessed. From wavelet analysis, the change in scale of grammage variation as a function of position was used to demonstrate regular and isolated differences in the formed structure.

1. Introduction

The study of paper variability is an essential element in monitoring the quality of paper production, diagnosing paper machine performance, and in developing effective machine design improvements. Advances in sensor and computational capabilities have motivated the search for new methods of analysis that will reduce paper variability data to meaningful results. This investigation made use of a novel approach, the *wavelet technique*, for use in distinguishing the local spectral characteristics, i.e. *simultaneous scale* and *space analysis*, of data obtained in the characterization of paper.

The analytical techniques based on the continuous wavelet transform were developed in the context of application to paper variability data, in earlier work by Keller *et al.*[2-4] Theoretical background was given, and analytical methods were justified using ideal trigonometric functions. The effectiveness of these analytical methods was assessed with closely controlled data sets that simulated the mass density, or formation, of paper. Representations of local spectral energy were determined for simulated paper images to determine the sensitivity of the method to variations in grammage, flocculation, gradient flocculation, and mean fiber orientation. To establish a frame of reference, samples were extensively character-

• Empire State Paper Research Institute, Faculty of Paper Science and Engineering, SUNY College of Environmental Science and Forestry, Syracuse, NY 13210.

ized by conventional statistical, formation and spectral analyses. The wavelet analysis developed in this investigation made use of the approach of Norman and Wahren[5] for the wavelength/formation spectrum, while extending characterization into the spatial dimension. As a concession for simultaneous scale-space representation, the wavelet transform gives lower spectral resolution as compared to the power spectra derived from the Fourier transform. The wavelet analysis showed susceptibility to individual features which tended to confound simple interpretation of the local energy maps. A solution was found in the consolidation of multiple spectral maps, determined from parallel lines within an image, so that local scale features of a one-dimensional non-stationary image could be represented.

The objective of this study was to apply the wavelet analytical methods to well controlled laboratory sheets and production samples, in order to explore the practical limits and sensitivity in the analysis of real paper formation. Sheet samples were selected to test the response to variation in grammage, flocculation, and mean fiber orientation.

2. Theory

A one dimensional wavelet transform was applied to data sets using a discrete implementation of the continuous wavelet transform. This method is non-orthogonal with relatively high redundancy in the convolution. Keller *et al.*[2] gave a thorough background of this approach. General and more comprehensive treatments of the wavelet technique are may be found in several texts[6], and articles.[7] The wavelet transform involves the correlation of the data set with a basis of analyzing functions derived from the dilation and translation of a single function referred to as the basic wavelet. The transform must meet several requirements to be considered a wavelet transform. First, the basic wavelet must integrate to zero and be localized in the spatial and frequency domain. In this investigation the second order Gaussian, or Marr wavelet, ψ_{G2}, was used as the basic wavelet. The function is given by:

$$\psi_{G2}(x) = \left(x^2 - 1\right)e^{-x^2/2} \tag{1}$$

The Fourier transform of this function, which is used in the analysis, is given as:

$$\hat{\psi}_{G2}(k) = -2k\,e^{-|k|^2/2} \tag{2}$$

The function is shown in Fig. 1. as represented in both the spatial and Fourier domains. A family of analyzing functions or wavelets is generated in the Fourier domain by the equation:

$$\hat{\psi}_{a,b}(x) = |a|^{1/2} e^{-2\pi w b}\hat{\psi}(aw) \tag{3}$$

where a and b are parameters used to scale and position the basic wavelet, respectively. These constitute a series of bandpass filters that are applied to the frequency spectrum of the data.

The continuous wavelet transform in the spatial domain is given by the relationship:

$$\tilde{f}(a,b) = |a|^{-1/2}\int dx\; f(x)\;\psi^*\left(\frac{x-b}{a}\right) \tag{4}$$

which results in an array of wavelet coefficients that represent an expansion of the original data set in the scale, as well as spatial domains. For the Marr wavelet, the resulting wavelet coefficients represent the amplitude of the local extrema of the data set.

It can be shown using Parseval' s theorem that the continuous wavelet transform in Fourier space is:

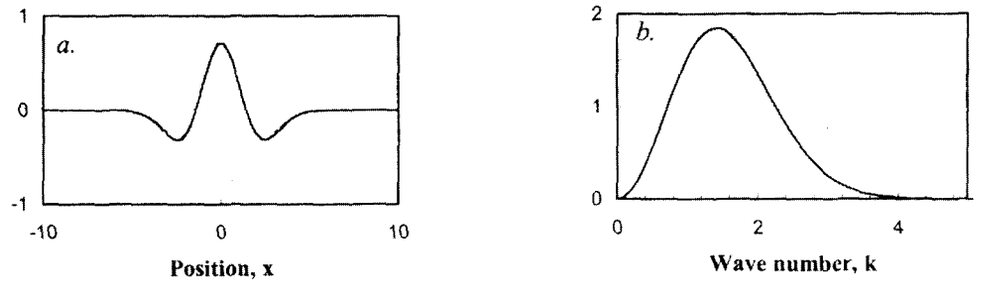

Fig. 1. Examples of the second order Gaussian function in the a) spatial domain, and b) Fourier domain.

$$\tilde{f}(a,b) = |a|^{1/2} \int dw\, e^{2\pi i w b} \hat{\psi}^*(aw) \hat{f}(w) \quad (5)$$

where $\hat{\psi}$ is given in Equation (2) and $\hat{f}$ is the Fourier transform of the data set.

The wavelet coefficients may be graphically represented in a two dimensional spectral plot of scale vs. position, referred to as a wavelet map. Wavelet maps indicate the amplitude of local maxima and minima, and since they are bipolar, they are best represented in color. In this report, contour maps are used to indicate the gradient between maxima and minima.

The local energy spectrum of the data set may be derived from the wavelet coefficients using the relationship:

$$E_{\psi G2}(a,b) = \frac{|\tilde{f}(a,b)|^2}{a\pi} \quad (6)$$

Squaring the wavelet coefficients results in a conversion from amplitude of the extrema to the localized energy. Normalization of the energy with the scale gives the wavelength spectrum familiar in formation analysis.[4] Maps of the local energy may also be represented in two-dimensional plots, sometimes referred to as scalograms, where for all cases, the results $E_{\psi G2} \geq 0$.

Composite local energy (CLE) maps were used to characterize feature scale and position simultaneously. Such maps were obtained by averaging fifty local energy maps that were determined for each image from parallel profiles spaced at 1 mm intervals. The common spectral information along the length of the profile is emphasized while the features unique to individual profiles are diminished. This approach assumes statistical stationarity in the direction perpendicular to the profiles.

The mean energy spectrum (MES) is derived by integration of the local energy spectrum in position at the various scale bands or octaves so that:

$$E_{\psi G2}(a) = \int_{-\infty}^{\infty} E_{\psi G2}(a,b)db \quad (7)$$

The resulting energy spectrum as a function of scale or wavelength and gives an approximation of the classical power spectrum as determined in Fourier analysis.[5] The mean energy spectra were determined from the composite local energy map by integration in space at each scale interval. In this study, the mean energy spectra and the wavelength/formation spectrum, which is a function of the power spectrum, were compared on plots of spectral density vs. wavelength.

3. Experimental

3.1 Materials

A series of isotropic hand sheets was obtained from the Pulp and Paper Centre, University of Toronto. The furnish consisted of bleached softwood Kraft pulp with a mean fiber length of 2.47 mm, width of 25 μm and a coarseness of 146 μg/m. Sheets were formed according to TAPP Standard 402. Grammages for the various samples are given in Table 2. The extent of flocculation was increased from standard isotropic hand sheets (*non-settled*) by introducing a two-minute settling time before drainage (*settled*).

Laboratory sheets with anisotropic mean fiber orientation were obtained from Weyerhaeuser Corp. The samples were prepared from western hemlock TMP with CSF of about 95 mL. Handsheets were made using a Formette Dynamique CD-300. Low and high levels of sheet anisotropy were made by varying the rotation rate and the deposition pressure. Sheet anisotropy was measured using an ultrasonic TSO-Tester (Lorentzen and Wettre). The two samples are identified in Table 1 where sheet forming conditions and sheet characteristics are given.

Table 1. Properties of Anisotropic Laboratory Sheets

	MD/CD Ratio	
	2.1	4.3
Mean Grammage (g/m^2)	58.75	57.49
Rotation Rate (rpm)	90	1500
Nozzle pressure (bar)	1.5	1.0

3.2 Methods

β-radiographs for the isotropic sheets were determined using the procedure described by Ng[8] which was based on earlier work by Cresson.[9] In this method, the paper sample was positioned in direct contact between a C^{14} radioactive source (11.9 mCi as a PMMA sheet) and X-ray film (Structrix D7, Agfa). Exposure time was 30 min. The β-radiographs were digitized using a flatbed transmission scanner (Scanmaker II, Microtek) set to a resolution of 0.1mm/pixel (254 dpi). An alternate method for radiographic imaging was used for the streaked and cross machine production samples. For these samples, latent transmission images were captured storage phosphor screens and directly digitized using a PhosphorImager SI (Molecular Dynamics, CA). A thorough discussion of this method is given elsewhere.[10] A 51.2×51.2 mm image was extracted from each digitized image and subsequently used in data analysis. Gray levels were assigned corresponding grammage values based on calibration using a step wedge of Mylar standards tested with each β-radiograph.

The electron beam transmission (EBT) was used to image the anisotropic handsheets. A detailed discussion of this method, based on the earlier work of Tomimasu[11], was presented by Keller and Luner.[12] The method used a transmission electron microscope (JEM-100S, JEOL) that was modified to allow the imaging of electron attenuation by paper sheets. Paper samples were placed in contact with a 7×7cm , $Ca(Eu)F_2$ crystal window that emitted visible light as a function of the intensity of electrons incident to the crystal surface (cathodoluminescence). As the sample was exposed to a field of 80 kV electrons, transmitted electrons formed a visible pattern on the crystal, representative of the in-plane distribution of mass within the sheet. A CCD camera was used to digitize the image for further analysis. Images were 51.2×51.2 mm with a resolution of 0.1 mm/pixel. The instrument was calibrated using Mylar film standards so that local

grammage could be determined from measured gray level values.

4. Results and discussion

4.1 Flocculation in isotropic laboratory sheets

The images obtained from beta radiographic imaging of the non-settled and settled laboratory sheets formed at various mean grammages are shown in Fig. 2. In comparing these images, the influence that settling had on increasing the "flocciness" of the formation structure is evident. The results from statistical analysis of the grammage maps derived from the beta radiographs are given in Table 2. The increased flocciness may be quantified by comparing all of the traditional formation parameters given in the table for each of the Non-settled and Settled samples.

Composite local energy (CLE) maps were generated from all of the isotropic sheet images. Fig. 3 shows the CLE maps for the non-settled and settled sheets prepared at 30 g/m^2 and measured by beta radiography. The increased flocculation after settling gave an increase in the spectral density at larger wavelengths while minimal change occurred at the finer scales. This suggests an increase in the content of larger scale flocs. Little change is apparent at the finer scales less than 0.5 mm. Generally, the trends observed in these plots are representative of those observed at the other mean grammages. Both the non-settled and settled plots show a mild artifact at the image edge that results from the aliasing of the wavelet transforms at the ends of the profile data. Consequently, interpretation of these plots should be limited to the central region of the map, from approximately 5 to 45 mm, that is unaffected by the edge effect. The plots in Fig. 3 also illustrate the occurrence of individual features that result from prominent flocs or lightweight zones in the images. They appear as small peaks that are aligned along the wavelength axis. By consolidating local energy maps to form composites, the effect of the local features is reduced so that underlying trends are revealed.

Fig. 4 shows the mean energy spectra for wavelet transforms for the 20, 30 and 60 g/m^2 images. By integrating the CLE maps, cf. Fig. 1, in space, an approximation of the wavelength/formation spectrum for each

Table 2. Statistical Analysis of Laboratory Sheets using β-Radiography

	Isotropic						Anisotropic	
	Non-Settled			Settled 2 min			MD/CD Ratio	
	20	30	60	20	30	60	2.1	4.3
Grammage (gravimetric)	20.0	30.5	65.5	20.3	30.7	64.3		
First Order Statistics								
Mean	20.1	30.2	63.3	19.4	35.5	63.7	59.1	58.6
Median	19	29	63	19	35	63	59	58
Std Dev	3.53	4.57	5.97	4.98	7.11	9.66	1.14	1.23
Variance	12.5	20.9	35.6	24.8	50.6	93.3	1.29	1.51
Covariance	17.6	15.15	9.44	25.7	20.1	15.2	1.92	2.10
Kallmes	1173	1118	609	704	455	342	2818	2798
Graininess	2.48	2.53	2.42	1.87	1.70	1.55	2.18	2.08

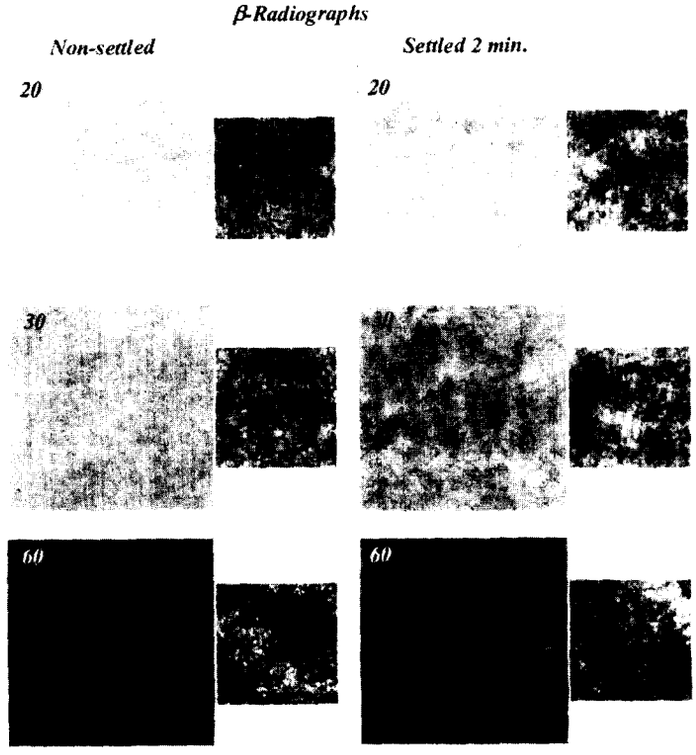

Fig. 2. β-radiographic images of the isotropic laboratory sheet samples. Images for non-settled (2 min) are shown. Samples are identified by approximate mean grammages.

image is represented. In this plot, the spatially independent trends observed in the CLE maps may also be clearly seen.

Local scale features are affected to a much greater extent by the flocculation than the fine scale. Conventional wavelength/formation plots are compared with MES in that Fig. The reasonable agreement between the two methods demonstrates the fidelity of the wavelet technique in estimating spectral density using the wavelength/formation spectrum as a reference. By comparing the MES of the non-settled, cf. Fig. 4a, and settled, cf. Fig. 4b, the increase in spectral density at larger wavelengths, apparent the CLE maps, is also evident as the slope of the curves increase with flocculation.

4.2 Orientation of anisotropic laboratory sheets

The images obtained by EBT imaging of the anisotropic laboratory sheets are represented in Fig. 5. Although the papers differ significantly in anisotropy, with MD/CD ratios of 2.1 and 4.3, this difference is not easily detected by inspection of the papers or the EBT images. Fig. 5 also includes the gray level enhanced enlargements that show details of the fine structure with the principle axis of orientations aligned vertically with the page. In the enlargements, the structure of the sheets is more clearly visible where a slightly higher orientation may be seen for the high anisotropy sample. The local grammage distributions for EBT

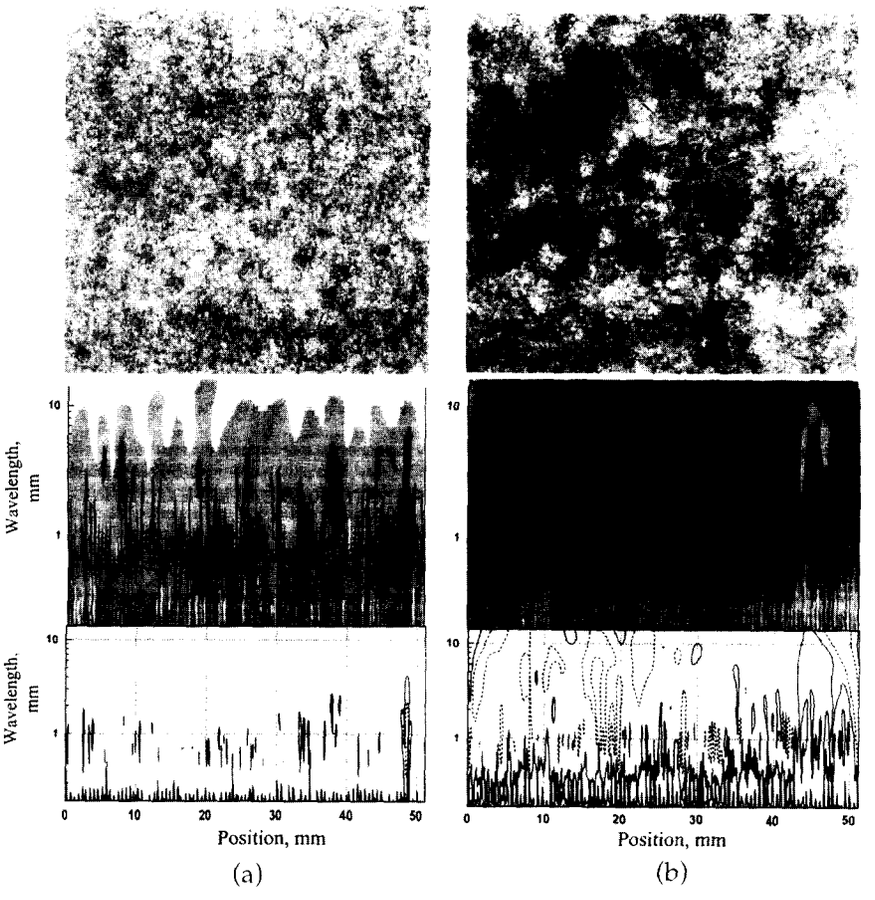

Fig. 3. Composite local energy (CLE) maps and β-radiographic images of the 30 g/m^2 isotropic laboratory sheets. Spectral plots illustrate the pattern of the energy maps. The contour plots demonstrate thresholding capability. Results for a) non-settled and b) settled (2 min) are shown.

images of these sheets (not shown) had narrow peaks spanning less than 10 g/m^2 and were effectively indistinguishable. The results of statistical analysis of the anisotropic samples are given in Table 4. The small differences that exist between the samples for most of the statistical parameters suggest a coarser floc structure in the high anisotropy sample.

Composite local energy (CLE) maps were created for the low and high anisotropy sheets. Since the current study is limited to one-dimensional wavelet analysis, CLE maps were compiled from profiles taken in both the machine and cross machine directions. In and earlier study[3] it was shown that wavelet analysis could be used to characterize the differences in feature scale in the machine and cross machine directions for anisotropic simulated formation images. Although these differences could be assessed using the wavelength/formation spectra, the wavelet analysis identifies the change in spectral density as a function of position. Fig. 6 presents the machine and cross machine CLE maps for the high

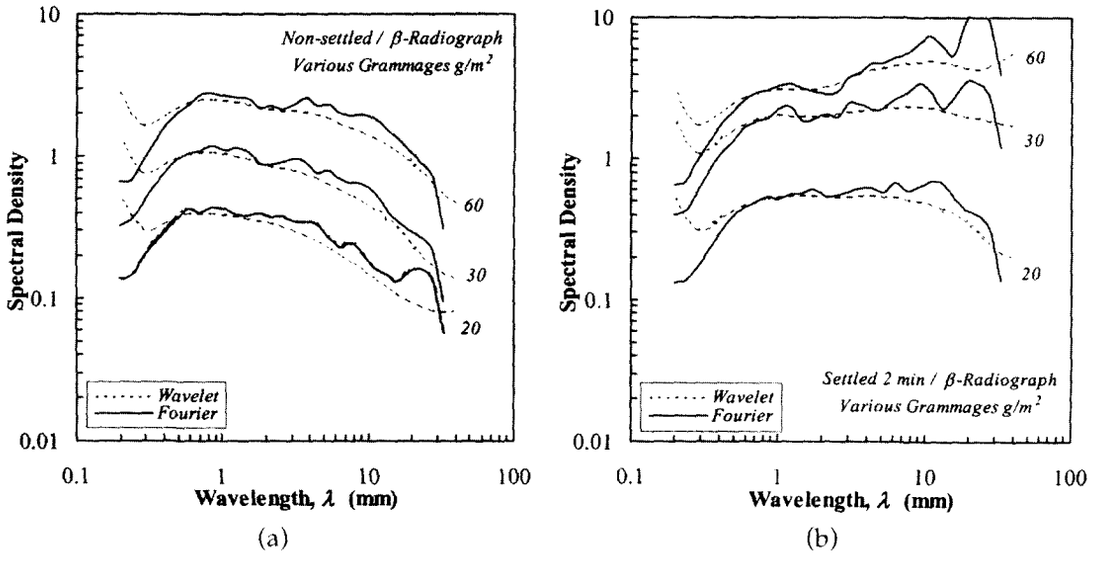

Fig. 4. Mean energy spectra (MES) and wavelength/formation spectra for the β-radiographic images at 20, 30 and 60 g/m². Results for a) non-settled and b) settled (2 min) are shown.

anisotropy laboratory sheet sample. Considering only the central regions in both plots, a maximum ridge of spectral density extends parallel to the position axis. The spectral density gradually decreases with increasing wavelength. The ridge in spectral density of the CD plot is formed at a lower wavelength than as seen in the MD plot. The relationship between these plots is similar to what was observed with the simulated formation images. This is, in effect, a quantification of the increased aspect ratio of the flocs aligned along the MD axis, cf. Fig. 5 enlargements.

Mean energy spectra formed from the CLE maps, shown in Figs. 7 and 8, clearly illus-

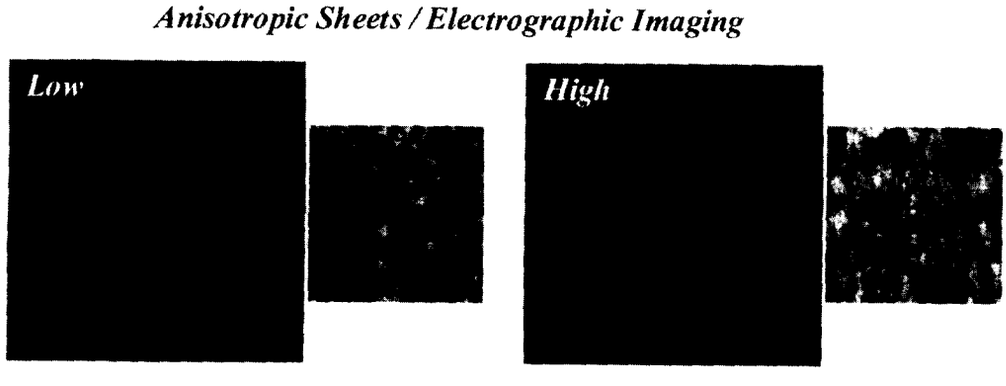

Fig. 5. EBT images of the anisotropic laboratory sheets. Adjacent images are the 3×magnification of the center 1 cm square that has been normalized by adjusting the graylevel histogram to enhance details.

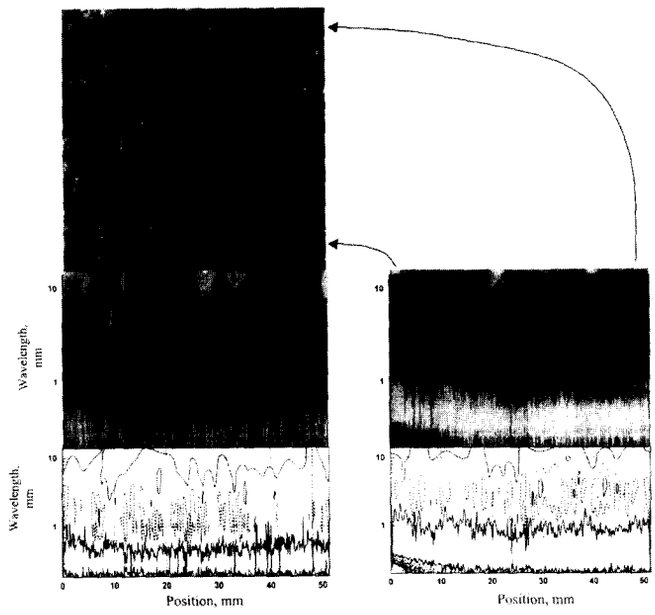

Fig. 6. Composite local energy (CLE) maps for the electron beam transmission images of high anisotropic sheet sample. Analysis orientation in the a) CD and b) MD are shown.

from the increase in grammage observed in the streak region, as compared to the rest of the sheet. Another consideration is that the local energy maps do not distinguish

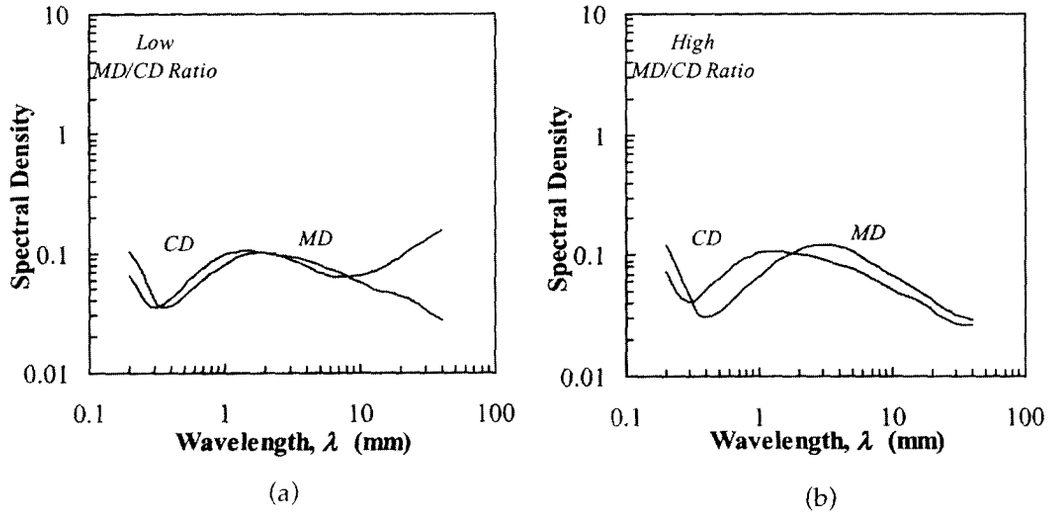

Fig. 7. Mean energy spectra (MES) for the EBT images of the a) low and b) high anisotropic laboratory sheets. Both MD and CD analysis orientations are shown.

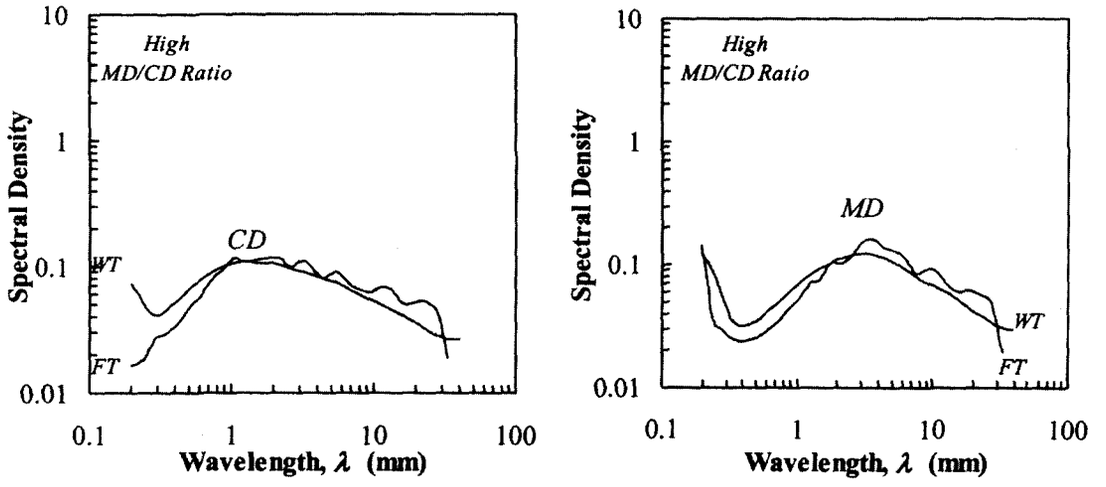

Fig. 8. Mean energy spectra(MES) and wavelength/formation spectra for the EBT images of the high anisotropic laboratory sheets. Analysis orientations in the a) CD and b) MD are shown.

trate the difference in the ridge for the MD and CD results as shown in Fig. 6. In Fig. 7, results from the low and high anisotropy sheets show the MD ridge to occur at larger wavelengths. It can be concluded that analysis using the wavelet transform has sufficient sensitivity to the change in floc size associated with sheet anisotropy. However, the presence of local features and local variation in formation demonstrated in the previous section, may preclude the ability to detect local variation in fiber orientation by this method. In Fig. 8, the MES and wavelength/formation spectra are presented for comparison. As with the isotropic samples discussed above, results from the two methods are in good agreement with the wavelength spectra providing greater spectral detail.

4.3 Product sample with streaks

A sample of unbleached Kraft liner facing made on a Fourdrinier former was obtained as an example of a sheet with heavy streaking. The sample measured 10 cm × 14 cm and had a mean grammage of about 80 g/m^2. The formation of the sheet was obtained using beta transmission with storage phosphor screens. The grammage array of the image was determined using the internal standards of the digitization image. Selected regions that extended in the cross machine direction were subjected to wavelet transform analysis.

The results were consolidated into composite local energy maps that are shown in Fig. 9. The two images that were analyzed were separated by about 8 cm, i.e. top and bottom of the sample held with MD positioned vertically. While streaks were apparent in the images, the CLE and contour maps provide additional information about the scale of the features within the streaks, and at other positions in the sample. Note that in the 8.0 cm region of the bottom sample, a cluster of peaks occurs with a wavelength of about 0.5 to 1.5 mm, whereas the regions at about 7 cm or at 12.0 cm have a deficiency of such features. Part of the response observed with these samples arises

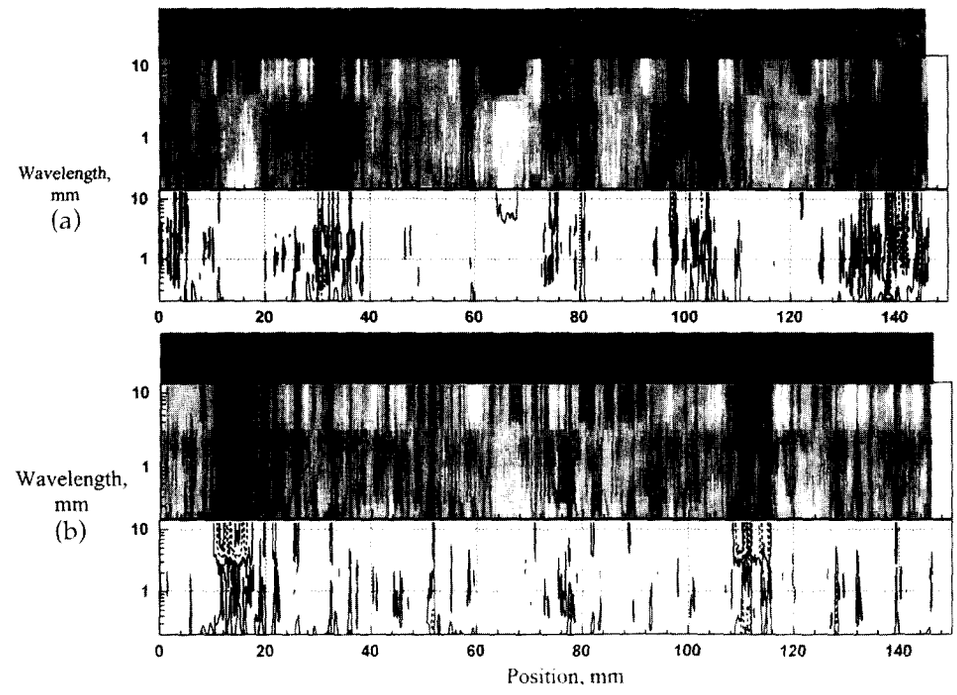

Fig. 9. Composite local energy (CLE) maps and β-radiographic images of the production sample with streaking. Spectral plots illustrate the pattern of the energy maps. The contour plots demonstrate where the local energy exceeds a threshold value. Results for two sections a) top and b) bottom of the sample sheet and are separated by 8 cm. The machine direction of the images is oriented vertically, and multiple one-dimension wavelet analyses were performed in the cross machine direction.

between the flocs and lightweight zones, but rather groups the features by scale.

5. Conclusions

A novel method for the analysis of one dimensional paper variability data for localized spectral density was developed. In earlier work by Keller *et al.*,[2-4] the wavelet technique was introduced and several analytical methods were discussed as applied to ideal trigonometric functions. The utility of the wavelet method for characterizing structural differences, such as grammage, flocculation and orientation were assessed. Data from statistically controlled reference images were used to evaluate the capabilities of the approach. This report presented the results from expanding the study to examine the applicability of the wavelet analysis for use with real laboratory sheet samples differing in grammage, flocculation and orientation.

Laboratory sheet samples were analyzed using electron beam transmission (EBT) imaging and β-radiography to acquire images representing the local distribution of mass (formation) of the sheets. The statistical and spectral analysis established the differences that existed between the samples using conventional descriptors.

The differences between the non-settled

and settled (flocculated) sheets could be distinguished using statistical, spectral and wavelet analysis. The wavelet analysis of the β-radiographic images gave clear differences for the range of grammages, and the flocculation step.

Anisotropic laboratory sheets were obtained at low and high orientation. At a MD/CD ratio of about 2.1, the differences between wavelet analysis in the MD and CD directions were very small. However, for the high anisotropy sample, with an MD/CD ratio of 4.34, the peak centers for spectral density were about 1 mm for CD and about 3 mm for the MD suggesting that the differences could be observed. It was also concluded that the relationships observed for the previously reported simulated images[3),4)] were viable in application to real paper formations.

Acknowledgement

The authors appreciate the assistance of Mr. W. Ng and Dr. C. J. T. Dodson from the University of Toronto, Dr. P. Lancaster, Weyerhaeuser Corp., and Dr. A. Kiviranta, Valmet Oy. The financial support of the Empire State Paper Research Associates is gratefully acknowledged.

Literature Cited

1. Presented at the TAPPI International Paper Physics Conference, September 26-30, 1999 San Diego, CA, TAPPI Press, Atlanta, 1999, pp. 357-369.
2. Keller, D. S., Lewalle, J., and Luner, P., "The Analysis of Paper Variability Using The Wavelet Transform", Paperi ja Pu, 81(6): 440-446, 1999
3. Keller, D. S., Lewalle, J., and Luner, P., "Wavelet Analysis of Simulated Paper Formation", Paperi ja Pu, 81(7):499-505, (1999).
4. Keller, D. S. in Paper Formation Measurement by Electron Beam Transmission Imaging and Analysis Using Wavelet Transforms, Ph.D. Thesis, SUNY ESF, Syracuse, NY (1996).
5. Norman, B., Wahren, D., "A comprehensive method for the description of mass distribution in sheets and flocculation and turbulence in suspensions", Svensk Papperstidning 20, 7 (1972).
6. G. Kaiser, in A Friendly Guide to Wavelets, Birkhauser, Boston, 1994.
7. M. Farge, J. C. R. Hunt, and J. C. Vassilicos, eds., Wavelets, Fractals, and Fourier Transforms, Clarendon Press, Oxford, 1993.
8. Ng, W. K., and Dodson, C. T. J., "Rapid Formation Performance Test", in Proceedings 1995 Int. Paper Phys. Conf, Niagara-on-the-Lake, ON, TAPPI Press, Atlanta (1995).
9. Cresson, T. M., Tomimasu, H., and Luner, P., "The Characterization of Paper Formation, Part I. Sensing Paper Formation", Tappi J., 73(7):153-159 (1990).
10. Keller, D. S. and Pawlak J. J., "Storage Phosphor Imaging of Paper Formation", J. Pulp Paper Sci., accepted for publication, April 2001.
11. Tomimasu, H., Luner, P., and Hanna, R. B., "Rapid Imaging of Mass Distribution in Paper by Electron Beams," Fundamentals of Papermaking, Vol. 1, Mechanical Engineering Publications, London, 159-194 (1989).
12. Keller, D. S. and Luner, P., "Measurement of Mass Distribution of Films and Fibrous Materials using Electron Beam Transmission", Rev. Sci. Inst. (1998).